Applied Catalysis B: Environmental 110 (2011) 186–194

Contents lists available at SciVerse ScienceDirect

Applied Catalysis B: Environmental

journal homepage: www.elsevier.com/locate/apcatb

An innovative electrochemical degradation of 1-diazo-2-naphthol-4-sulfonic acid in the presence of $Bi_2Fe_4O_9$

Lin Gu, Fan-Yong Song, Nan-Wen Zhu*

School of Environmental Science and Engineering, Shanghai Jiao Tong University, Shanghai 200240, China

ARTICLE INFO

Article history:
Received 27 July 2011
Received in revised form 29 August 2011
Accepted 31 August 2011
Available online 7 September 2011

Keywords:
Electrochemical degradation
Gas-diffusion electrode
1,2,4-Acid
$Bi_2Fe_4O_9$

ABSTRACT

This paper explores the degradation of a model pollutant, 1-diazo-2-naphthol-4-sulfonic acid (1,2,4-Acid), by an advanced oxidation process that combines electrochemical degradation and $Bi_2Fe_4O_9$ (BFO) oxidation. Experiments were done using a gas-diffusion cathode to produce in situ hydrogen peroxide by oxygen reduction. Column crystal semiconductor $Bi_2Fe_4O_9$ was synthesized and used as a novel catalyst in the combined system. It was characterized by X-ray diffraction (XRD), scanning electron microscopy (SEM) and transmission electron microscopy (TEM). Comparative experiment in two separated systems (BFO/H_2O_2 and BFO/Electrolysis) was conducted to determine the mechanism involved in the process. The effect of operating conditions such as applied current, solution pH, catalyst dosage on the efficacy of the process was investigated. It is shown that 1,2,4-Acid and its products can be effectively degraded by the $OH^{\bullet}$ radicals produced by the reaction between BFO and the electro-generated H_2O_2, which was further being confirmed with the electron spin resonance spin-trapping technique. Hydroxyl radicals generated in the process that led to the complete and rapid elimination of total organic carbon was observed even at low catalyst loadings. In this system, almost a complete removal of COD (89%) was achieved after 200 min using 1.0 g L^{-1} of BFO, whereas at the same time, only 39% and 32% of COD was removed by an individual process alone (electrochemical degradation and BFO adsorption, respectively). In this combined system, BFO has the principle role of adsorbing the initial substance on the surface of catalyst and catalyzing the electro-generated H_2O_2 to form active hydroxyl radicals. The LC-(ESI)-TOF-MS analysis indicated that the mineralization occurred simultaneous with the destruction of naphthalene ring, and 1,2,4-Acid was oxidized to colourless intermediates (mainly phthalic acid, small carbonyl species) and then to carbon dioxide.

1. Introduction

Water pollution by persistent and non-biodegradable organics substances such as dyes imposed a serious threat to the living species on the earth. Nowadays, the dye processing industries are available in developing countries, so large volumes of wastewater generated from the dye processing industries containing suspended solids, unreacted dyestuffs, and other auxiliary chemicals have been causing deteriorating natural environment. For instances, the presence of 1,2,4-Acid, a naphthalene dye intermediate, is hazardous for human beings in discharged water for its carcinogenic effect.

Recent results have shown that advanced oxidation processes (AOPs), which are based on the formation and use of the extreme oxidant hydroxyl radicals, offer promising alternatives for removal of chemical contamination in water [1–3]. The common way to make hydroxyl radicals is to inject acidified solution of ferrous ions into the wastewater, followed by concentrated H_2O_2. This is the well-known Fenton reaction: [4]

$$H_2O_2 + Fe^{2+} \rightarrow Fe^{3+} + {}^{\bullet}OH + OH^- \quad (1)$$

The electrochemical oxidation of organics for wastewater treatment can be obtained by direct electrolysis, where the pollutants are oxidized after adsorption on the anode surface without the involvement of any substances other than the electron. Direct electro-oxidation is theoretically possible at low potentials, before oxygen evolution, but the reaction rate usually has slow kinetics and a decreased catalytic activity due to the formation of polymer layer on the anode surface [5,6]. Another approach to the electrochemical treatment of organic pollutants is the indirect electrolysis generating in situ chemical oxidizing agents to react with the pollutants, such as chlorine and hypochlorite and hydrogen peroxide. However, it is commonly accepted their use might lead to the formation of organochlorinated compounds.

On the contrary, hydrogen peroxide is an environmental friendly reagent that leaves no hazardous residuals and can be decomposed

* Corresponding author. Tel.: +86 21 54742817; fax: +86 21 34203732.
E-mail address: nwzhu@sjtu.edu.cn (N.-W. Zhu).

0926-3373/$ – see front matter © 2011 Elsevier B.V. All rights reserved.
doi:10.1016/j.apcatb.2011.08.042

to hydroxyl radicals via the reaction (1). Hydrogen peroxide can be electrogenerated in acidic solutions by electro reduction of oxygen on the cathode surface:

$$O_2 + 2H^+ + 2e^- \rightarrow H_2O_2 \quad (2)$$

More recently, gas diffusion cathodes (GDE) have demonstrated to be promising electrode materials for the electrogeneration of H_2O_2 from oxygen reduction [7]. Previous literatures have reported the application of H_2O_2 electrogenerated on GDE for the treatment of the wastewater containing organic pollutants in the presence of Fe^{2+} ions [8] or with Fe^{2+} and UVA irradiation (photo-assisted electro Fenton process) [9]. Unfortunately, the formation of a significant amount of ferric hydroxide sludge in the course of Fenton treatment, and the requirements of further separation and disposal for the resulting sludge limit the use of the process.

Heterogeneous Fenton-like catalysts have recently attracted much more attention, such as iron oxide [10], and iron-immobilized zeolite [11], clays [12], and carbon materials [13]. Relative to homogeneous Fe^{2+} catalyst, these heterogeneous catalysts can treat organic pollutants in a wide pH range and leave no hazardous residuals like ferric sludge. However, many of them are applied in the commercial hydrogen peroxide induced heterogeneous Fenton-like system, and always do not show favorable activity.

As we know, BFO are important heterogeneous catalysts in industrial reactions [14,15], and can also function as a catalyst in photo catalysis, and limited data have been published on 1,2,4-Acid degradation and mineralization by AOP. Based on our previous study of electrochemical induced catalytic oxidation of wastewater in the presence of transition metal modified catalyst [16], herein, we studied the performance of BFO as a novel catalyst in the electrochemical induced catalysis system. The application of BFO in the electrochemical induced system using GDE has not been reported so far. The present work is aimed at providing insight into the catalytic ability of BFO in the combined system. 1,2,4-Acid is selected as a model pollutants and its degradation pathway in this coupled system is illustrated. A proposed degradation mechanism in the combined electrochemical system with BFO is also depicted and verified by the ESR technique.

2. Experimental procedure

2.1. Chemical and materials

All chemicals were prepared using deionized water from a Millipore system with a resistivity of 18.2 MΩ cm. Iron nitrate ($Fe(NO_3)_3{\cdot}9H_2O$), bismuth nitrate ($Bi(NO_3)_3{\cdot}5H_2O$), NaOH and HNO_3 were obtained from Shanghai Chemical (Shanghai, China). 1,2,4-Acid was provided by Sanfeng Chemical Reagent Co., Ltd (Shanghai, China). The wastewater was simulated by dissolving 500 mg L^{-1} 1,2,4-Acid to the distilled water and its initial COD was 710 mg L^{-1}. All chemicals were analytical grade reagents and were used as received without further purification.

2.2. Preparation of spinal crystal BFO

Typically, 1 mmol of $Bi(NO_3)_3{\cdot}5H_2O$ and 2 mmol of $Fe(NO_3)_3{\cdot}9H_2O$ were dissolved into 2 mL of HNO_3 (1 M). Then a concentrated aqueous solution of NaOH was added dropwise into the above solution until the pH value of the suspension was 13.5. After being stirred for 2 h, the suspension was transferred into a 50 mL Teflon-lined stainless steel autoclave up to 80% of the total volume. The autoclave was heated at 180 °C for 48 h at an ambient magnetic field, and then cooled to room-temperature naturally. The resulting samples were separated by filtration, washed with deionized water and absolute alcohol several times, and then dried at 60 °C for 12 h.

2.3. Characterization of catalyst

The particle size and morphology were examined using scanning electronic microscopy (SEM). The vacuum-dried samples were used for SEM analysis, which was carried out on a Quanta 200 (Holland) electron microscope combined with energy dispersive X-ray spectroscopy (EDXS) for element mapping (Phillips-FEI, 30 KV). TEM measurements were carried out on a CM20 (Philips) electron microscope, operated at 200 kV (point-to-point resolution, 0.24 nm). X-ray diffraction (XRD) measurements of the catalyst powder were recorded using D/Max-3c (Janpan Rigalcu) diffractometer equipped with Ni filtered Cu KR radiation (λ = 1.5406 Å). For electron spin resonance (ESR) assay, 100 μL samples were collected form the 1,2,4-Acid degradation system within 5 min and immediately mixed with 20 μL of 0.2 mol L^{-1} DMPO to form DMPO-•OH adduct, and the EPR spectra were obtained on a Bruker ESR 300E with microwave bridge.

2.4. Degradation experiment

The degradation experiments were carried out in an undivided cell with a volume of 250 mL, supplied with a heat exchanger and a magnetic stirrer under galvanostatic conditions using an AMEL 2055 potentiostat. The GDE was used as cathode electrode, a Ti grid with an area of about 5 cm^2 as anode. The electrode was fed with air at a flow rate of 20 mL s^{-1}. The gas flow passed over the inner face of the cathode through the tube inside the holder, the top of which was connected to a drechsel to maintain the right pressure in the Plexiglas holder. A stirrer was driven by magnetic stirrer apparatus at the agitation speed 300 rpm. All the experiments were conducted in the dark unless specified otherwise.

BFO was dispersed into 500 mg L^{-1} aqueous solution of 1,2,4-Acid without any control during the degradation. If not specifically mentioned, the degradation reaction was initialed by switching the power and adding 1.0 g L^{-1} BFO catalyst under magnetic stirring conditions.

All the experiments were repeated three times, and the results are the average of at least three measurements with an accuracy of ±5%.

2.5. Analyses

Evaluation of electrolysis and its combined effect with BFO was conducted. Solution samples were taken at a given time intervals during the reaction, and immediately centrifuged at 14,000 rpm for 3 min using an EBA-20 (Hettich, Germany) to remove BFO.

The wastewater was characterized for COD. For COD measurement, the samples were left overnight to remove the residual hydrogen peroxide that might remain in the sample solutions. Hydrogen peroxide concentration was determined by potentiometric titration using a standardized $KMnO_4$ 0.01 N solution in an automatic 702SM Metrohm titrator

Organic byproduct identification was carried out by means of Liquid Chromatography-(Electrospray Ionization)-Time of Flight-Mass Spectrometry (LC-(ESI)-TOF-MS) analysis of the different Fenton treated samples. Solid-phase extraction (SPE) with oasis HLB cartridges from Waters was employed for samples preconcentration prior to the analysis. Separation was made using reversed phase liquid chromatography (flow rate 0.5 mL/min, injection volume 20 μL) in a HPLC (Agilent series 1100) equipped with a 150 mm × 4.6 mm C-18 analytical column of 5 μm particle size. The column temperature was 25 °C.

Current efficiency (CE) for anodic oxidation of 1,2,4-Acid was calculated from COD values, using the following relationship:

$$C.E.(\%) = \frac{(COD_0 - COD_t)}{8 \times I \times t} F \times V \times 100 \quad (3)$$

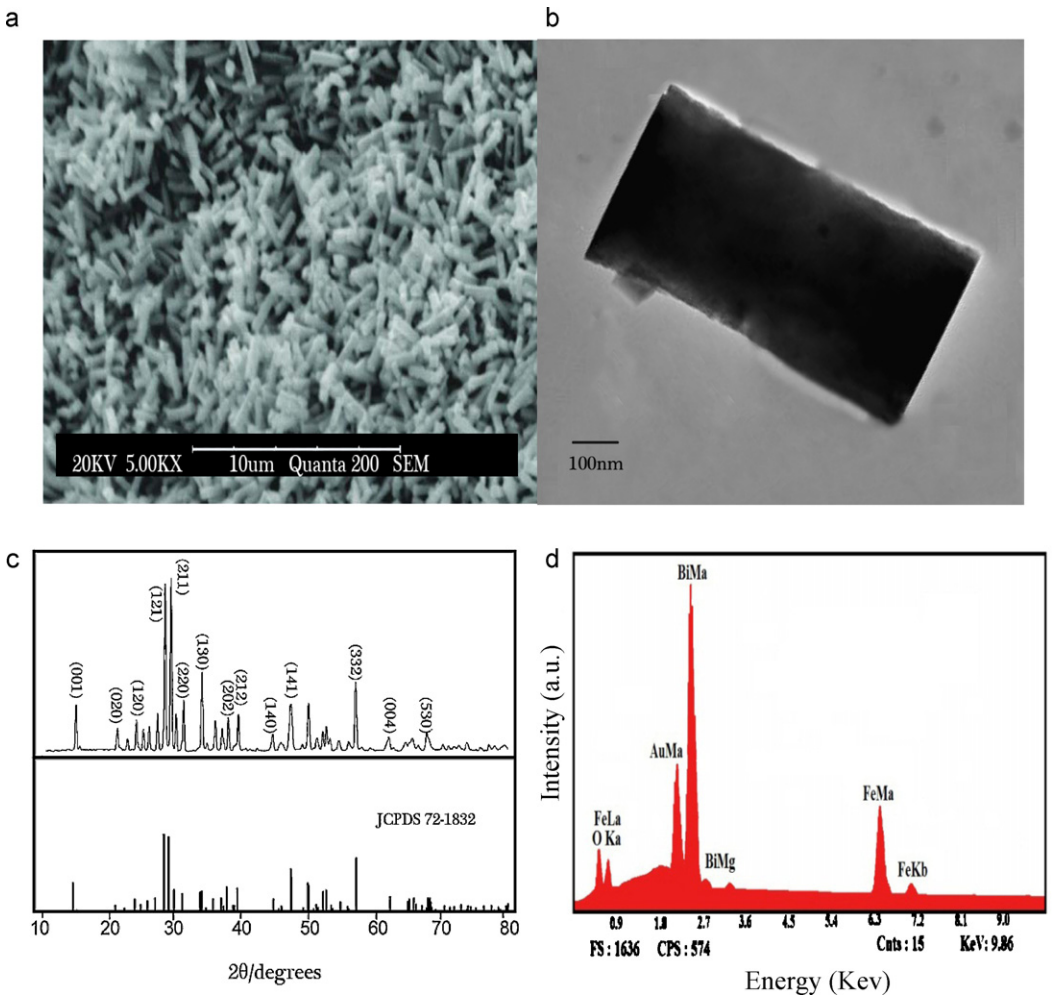

Fig. 1. Characterization of BFO catalyst. (a) SEM image, (b) TEM image, (c) XRD pattern, (d) EDS pattern.

where COD_0 and COD_t are chemical oxygen demands at times $t = 0$ (initial) and t(in g_{O_2} L) respectively, I is the current (A), F is the Faraday constant (96,487 C mol^{-1}), V is the electrolyte volume (L), and 8 is the oxygen equivalent mass (g eq^{-1})

3. Results and discussion

3.1. Characteristic of catalyst

The SEM observation indicated that BFO consisted of spinal crystal with diameters about 500 nm and with the length of 2–3 μm (Fig. 1(a)), and had uniform dispersion. It showed a spinal-like appearance with different side lengths along the perpendicular directions. A TEM image of a peeled fragment from the spin is shown in Fig. 1(b). It can be seen that the nano-plates are rectangle-like with different side lengths along the perpendicular directions. The XRD pattern (Fig. 1(c)) showed a highly crystalline and single phase. All of the diffraction peaks can be well indexed to orthorhombic $Bi_2Fe_4O_9$ (space group *Pbam* (55), JCPDS 72-1832). No other possible impurities can be detected. Fig. 1(d) gives EDXS elemental composition signals associated with the total image, strong signals in the total image correspond to O, Bi and Fe, the peak corresponding to Au comes from the coating for enhancing conductivity of the sample for SEM.

3.2. 1,2,4-Acid removal in different systems

To identify the individual contribution of each process (electrolysis/BFO adsorption/BFO-electrolysis), the systems were tested separately. Fig. 2(a) shows H_2O_2 yield with the function of time in the absence of BFO catalyst. It is seen that $Y(H_2O_2)$ increases with the increase of electrolysis time while the flow rate of the air is controlled at 20 mL L^{-1}, and the higher air flow in excess of the optimal value did not bring about the enhancement of $Y(H_2O_2)$ (data not shown), which agrees well with oxygen reduction behavior described in literature [17]. The 200 min H_2O_2 yield is 17 mg L^{-1}.

Fig. 2(b) shows the COD variation of 1,2,4-Acid versus time under different conditions. In these systems, combined results for COD reduction were better than both obtained in electrolysis and BFO adsorption. It is seen that the COD removal of 1,2,4-Acid by BFO adsorption was 32%. It is well known that surface area greatly affects its catalytic activity [18]. 1,2,4-Acid on BFO displayed the characteristic of Freundlich-type isotherm (Eq. (4)), suggesting the sorption onto the heterogeneous surface. Regarding the correlation coefficients, the experimental data fit Freundlich isotherm ($r^2 = 0.969$) better than Langmuir isotherm ($r^2 = 0.924$).

$$\log qe = \log Kf + \frac{1}{n}(\log Ce) \quad (4)$$

Synthesized BFO particles in this article have more micro-sized spinal-like crystals, the intersections of parallel or crossing spinals

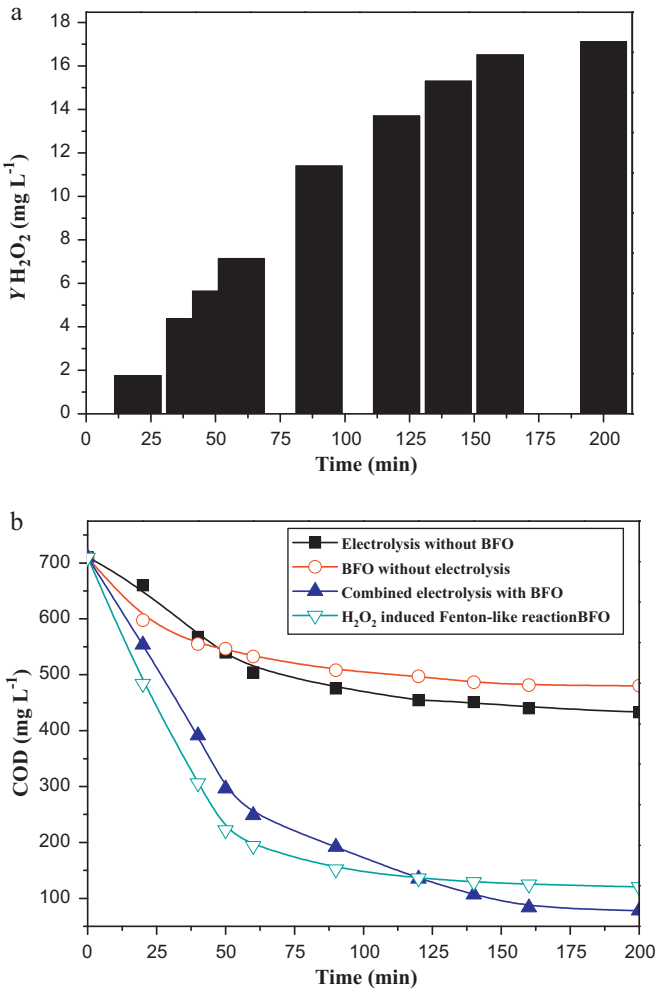

Fig. 2. (a) H_2O_2 yield with the function of time in the electrochemical system without BFO particles using GDE as cathode. Conditions: pH 5; $T = 25\,^{\circ}C$; Current density = 40 mA cm^{-2}; electrode distance = 30 mm; (b) COD elimination by electrolysis, BFO adsorption, BFO/Electrolysis combined process and BFO/H_2O_2 combined process. Conditions: pH 5; $T = 25\,^{\circ}C$; Current density = 40 mA cm^{-2}; electrode distance = 30 mm; BFO dosage = 1 g L^{-1}.

led to the pored structure (Fig. 1), which is benefit for 1,2,4-Acid physisorption onto the BFO particles. The Brunauer–Emmett–Teller (BET) measurements show that the surface area of the spinal-like $Bi_2Fe_4O_9$ is 12.2 $m^2\,g^{-1}$. The significantly larger surface area of BFO particles further results in the higher efficiency of 1,2,4-Acid adsorption.

Moreover, the isoelectric point of BFO was determined to be pH 6.9 according to the measurement of zeta potentials (Data not shown). Thus, the surface of BFO are positively charged, 1,2,4-Acid is dominantly present in the form of negative ions, and 1,2,4-Acid is easily adsorbed on the surface of BFO via electrostatic interaction at pH 5.0, this was also verified by Zhu et al. [19].

It is found that COD was removed by catalyst adsorption more rapidly than by electro-catalysis. However, the two processes were not environmentally equivalent due to the accumulation of unconverted contaminants on the solid phase by adsorption. In the absence of BFO, only 39% of COD depletion was obtained after 200 min of electrolysis because the main oxidant was the electrogenerated H_2O_2 that has limited oxidation power. In contrast, in the solution with BFO, 1,2,4-Acid oxidation was accelerated and the 200 min COD removal had increased to 89%, which might be due to the formation of $OH^{\bullet}$ radicals through the reaction of BFO and electrogenerated hydrogen peroxide.

Comparative experiments of two systems (BFO/H_2O_2 and BFO/electrolysis) were carried out. Amount of H_2O_2 added (17 mg L^{-1}) in the BFO/H_2O_2 system equals to the total concentrations of hydrogen peroxide accumulated in 200 min electrolysis time. The result is shown in Fig. 2(b), which indicates a better COD removal efficiency in the combined BFO/electrolysis system. However, it is observed that the 200 min COD removal efficiency could still be reached 83% in BFO/H_2O_2 system, which should be attributed to the activation of H_2O_2 in the presence of BFO particles. The decomposition of H_2O_2 in BFO/H_2O_2 system may involve the initial formation of hydroxyl radicals, which is known as Fenton-like reactions. The mechanism is in accordance with the observations on the literatures [10–13], which reported that iron oxide could catalyze the activation of H_2O_2 to produce $^{\bullet}OH$ radicals. The improvement in COD removal efficiency in BFO/electrolysis system is probably because that the H_2O_2 is generated continuously. This avoids the side reaction that excessive H_2O_2 can induce $^{\bullet}OH$ radicals scavenging effect. Generally, the large initial input of H_2O_2 needs shorter reaction time for the degradation of parent pollutants but achieves a relatively low COD removal efficiency, which was also confirmed in literature [20].

Table 1 shows the COD removal efficiency in each individual process, the results suggested a great enhancement of COD reduction in combined system with 89% of COD removal after 200 min treatment, whereas only 39% and 32% of COD removal were achieved in electrolysis and BFO adsorption separated processes. The trend of ICE with reaction time during the electrochemical process is also shown in Table 1. It can be seen that the ICE of electrochemical degradation with BFO particles is much higher than that without it, which might be due to the interaction of both electrochemical degradation and BFO. In combined systems, the BFO particles served as micro-electrodes, on which electrogenerated hydrogen peroxide might be decomposed through the catalytic effect of BFO catalyst. It should be noted that ICE higher than 100% in the combined system were possible in this study since COD removal was not only attributed to electro-catalyzed oxidation. The other reaction that also removes COD is adsorption with BFO particles. By this way, the COD will absorb on BFO particles, thus leading to the decrease in COD remaining in the solution.

3.3. Effect of pH

To clarify the effect of pH, dye solution with initial pH of 2.0, 3.0, 4.0, 5.0 and 6.0 were electrolyzed at 200 mA and the results are illustrated in Fig. 3.

A notable pH effect was found for the multi phased electrochemical degradation process, reaching its faster degradation at pH 3.0 with a maximum COD removal 91% at 200 min. This result is entirely consistent by the one reported by other authors [21] for the degradation of organic pollutants by electro-Fenton method and it is also very close to the optimal pH of 2.8 for Fenton's reaction [22].

However, distinct from traditional electro-Fenton processes, the reaction with electro-assisted BFO particles could occur over a wide pH range. The 89% of COD removal efficiency can be also achieved when the initial pH was 5. The decreased COD removal at pH ranging from 4 to 5 is probably due to that the eletrogenerated hydrogen peroxide is inhibited, as previously reported that the optimal pH range for H_2O_2 production is in acidic or alkaline pH region [16]. At pH above 6.0 the decomposition rate decreased because the oxidation potential of hydroxyl radicals decreases and the electrogenerated H_2O_2 is more easily decomposed to H_2O and O_2 with increasing pH [23] (Eq. (5)).

$$H_2O_2 \rightarrow 2H_2O + O_2 \quad (5)$$

While at very acidic pH, below pH 3.0, the electrogenerated hydrogen peroxide solvates a proton to form an oxonium ion

Table 1
Comparative results on the COD removal and ICE during the 1,2,4-Acid degradation by different processes.

Time (min)	Electrolysis		BFO adsorption	Electro-catalysis with BFO combined process	
	COD removal efficiency (%)	ICE (%)	COD removal efficiency (%)	COD removal efficiency (%)	ICE (%)
20	7.1	62.4	15.8	22	196.2
40	20.8	89.3	21.8	44.9	200.1
60	29	86.2	25	65	193.2
120	36	53.5	30	81	120.4
140	36.4	46.4	31	85	108.3
160	38	42.3	32	88.3	98.4
200	39	34.8	32	89	79.4

($H_3O_2^+$) that enhances its stability and reduce the reactivity with BFO and consequently less hydroxyl radicals are produced [24]. Moreover, dissolved ferric ions are easily leached at low pH region and thus get BFO deactivated, no leaching of Fe ions from BFO was detected at pH 5.0 and pH 4.0 because the concentration of Fe from BFO at this pH value was below the detection limit of the used methods (DL (Fe) = 4.0×10^{-3} mg L^{-1},). At pH 3.0, the concentration of leached Fe ions 0.856 mg L^{-1} was found by using ICP-MS method.

3.4. Effect of applied current

The influence of current density on 1,2,4-Acid oxidation has been investigated in the range 100–200 mA and the results are shown in Fig. 4.

These data show a gradual increase in COD removal rate with raising current. This enhancement of the oxidation power can only be associated with a greater production of H_2O_2 from reaction (5) leading to the generation of higher amount of hydroxyl radicals from BFO catalyzed reaction. In fact the current efficiency was almost independent on applied current and depends only on the specific charge passed. Fig. 4(inset) also shows that during the electrolysis the efficiency always undergoes a dramatic fall due to the gradual formation of intermediates that are destroyed with more difficulty, such as from aromatic to aliphatic structure by the ring-opening reaction [25]. At the same time, more oxygen evolution produced at anode simultaneously with the increase of current density which also leads to the decrease of ICE.

$$O_2 + 2H^+ + 2e^- \rightarrow H_2O_2 \quad (6)$$

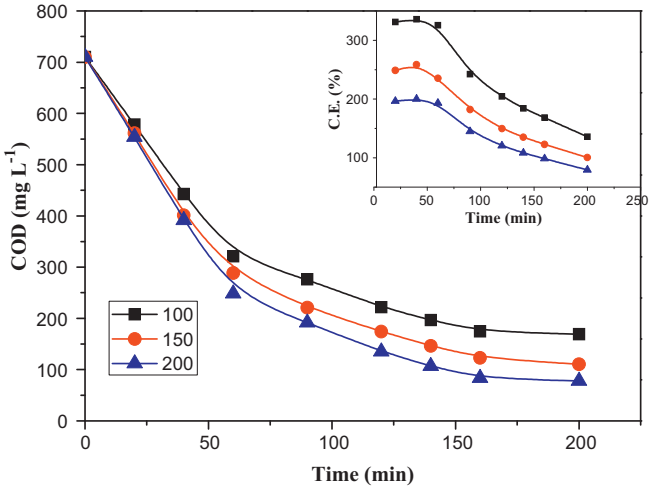

Fig. 4. Effect of applied current on COD and current efficiency (inset) evolution during the electrocatalysis of 1,2,4-Acid in the presence of BFO particles. Conditions: T = 25 °C; initial pH 5; electrode distance = 30 mm; BFO dosage = 1 g L^{-1}.

3.5. Effect of BFO dosage

Generally, higher reaction rate of electro-catalytic degradation are expected by increasing the catalyst dose. Fig. 5 shows the effects of BFO loads on the combined electrochemical degradation of 1,2,4-Acid. It was found that the COD removal rate increased with the increase of catalyst dose, indicating that higher loads of BFO result in a faster degradation. As can be seen from Fig. 5, the time required to attain 78% of the COD removal was 140 min and 200 min, respec-

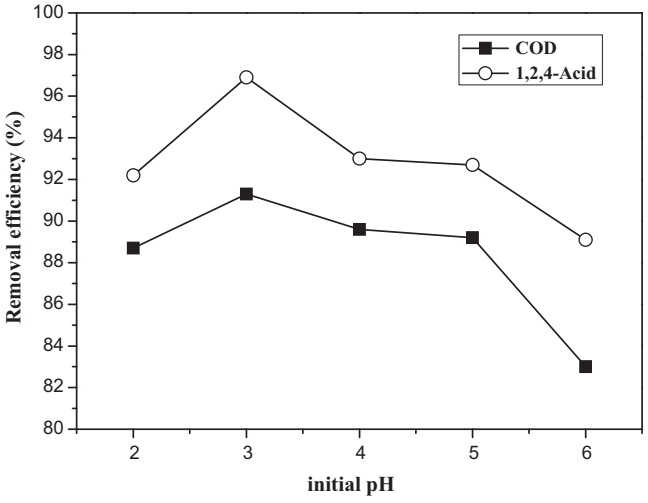

Fig. 3. Effect of pH on the 1,2,4-Acid and COD removal during the electrolysis of 1,2,4-Acid in the presence of BFO. Conditions: T = 25 °C; Current density = 40 mA cm^{-2}; electrode distance = 30 mm; BFO dosage = 1 g L^{-1}.

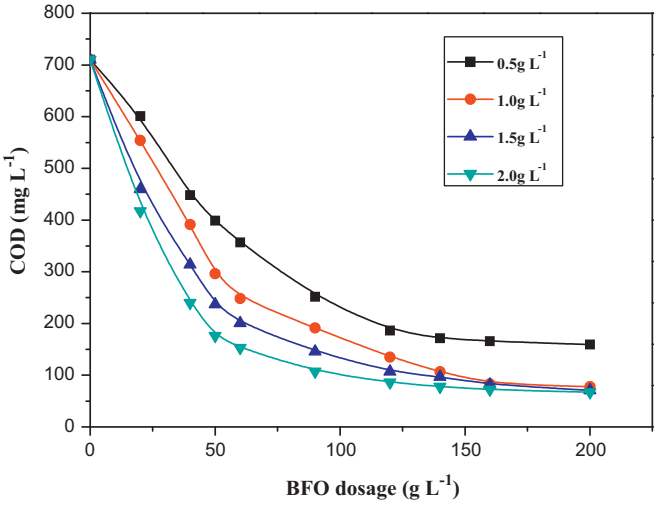

Fig. 5. Influence of the BFO dosage on the COD evolution during the electrocatalysis of 1,2,4-Acid in the presence of BFO particles. Conditions: T = 25 °C; Initial pH 5; electrode distance = 30 mm; Current density = 40 mA cm^{-2}.

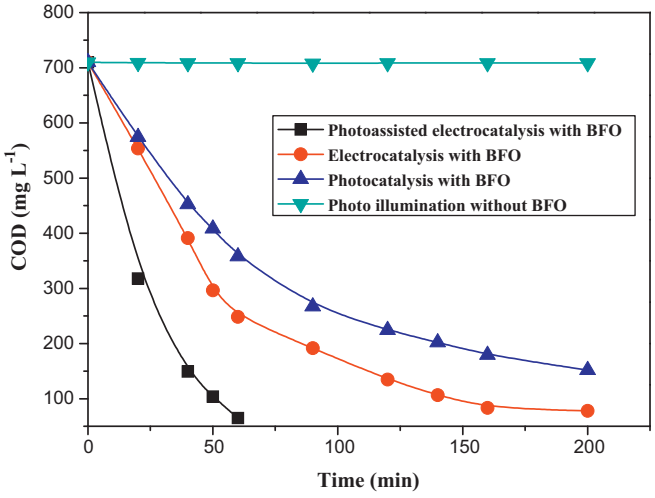

Fig. 6. Comparative results of COD evolution in four different catalytic systems. Conditions: $T = 25\,^{\circ}C$; Initial pH 5; electrode distance = 30 mm; Current density = 40 mA cm^{-2}; BFO dosage = 1 g L^{-1}.

tively, when 2 g/L and 1 g/L BFO catalyst was applied. However, almost the same removal efficiency was achieved when time prolonged indicating that the small molecular intermediates absorbed on the BFO surface might eventually undergo a mineralized degradation through the hydroxyl radicals. Based on both technical and economic reasons, the optimal BFO dosage should be chosen as 1 g L^{-1} in the electro-assisted catalytic process.

3.6. Photo-assisted electrocatalytic degradation of 1,2,4-Acid in the presence of BFO

As reported previously, BFO can function as a catalyst for photocatalysis [26]. In this section, heterogeneous catalyst BFO was employed in different conditions. Photocatalysis experiments were studied by using an irradiation source (300 W Dy lamp) and a 420 nm cutoff filter ($\lambda > 420$ nm), and the reaction temperature were kept at 25 °C by using an air conditioner. Control experiments were also made with and without the BFO particles under visible light illumination in order to prove photocatalytic performance of spinal-like BFO particles. The comparative result is shown in Fig. 6.

As can be seen, no degradation was observed when only visible light illumination was applied but a 78.6% of COD removal efficiency was achieved in the presence of BFO when the solution was irradiated by visible light. It reveals that 1,2,4-Acid is stable under short time visible light irradiation if there is no photocatalyst involved. In other words, the spinal-like $Bi_2Fe_4O_9$ particles are active to visible irradiation while the normal photocatalyst TiO_2 only responds to UV irradiation.

In the electrocatalysis systems with BFO, the introduction of photo irradiation significantly enhanced the degradation efficiency of COD. A 60 min COD removal efficiency had reached 99%. Previous literature reported that the Fenton degradation of organic dyes can be greatly accelerated under visible light irradiation [27], it is consistent with the results obtained in our photo-assisted combined electrochemical systems. The degradation lifetimes for 1,2,4-Acid are significantly shorter in the combination experiments than the ones observed in either the photocatalysis or electrocatalysis experiments with BFO. Experiments data reveals that the introduction of visible illumination into the aqueous suspension of BFO in the electrochemical system can result in enhanced photocatalytic activity, probably ascribed to the combined effect of photocatalysis of BFO and the Fenton-like reaction by electro-generated H_2O_2. Optical transition produced oxygen holes on the surface of catalyst functioned as oxidizers to oxidize H_2O and organics to hydroxyl radicals and organic intermediates directly:

$$H_2O + BFO(h^+) \rightarrow {}^{\bullet}OH \quad (7)$$

$$RH + BFO(h^+) \rightarrow R^- \quad (8)$$

Besides, optical transition induced electrons on the surface of BFO particles scavenger electro-generated H_2O_2 in the photoreaction system, electron–hole recombination could be effectively prevented, and offer extra hydroxyl radicals in order to improve the degradation efficiency (Eq. (9)):

$$H_2O_2 + Bi_2Fe_4O_9(e^-) \rightarrow {}^{\bullet}OH + OH^- \quad (9)$$

Moreover, electro-generated O_2 diffused on the surface of BFO particles can be reduced to $HO_2^{\bullet}$, which could react with itself to produce hydrogen peroxide (Eq. (11)):

$$O_2 + Bi_2Fe_4O_9(e^-) + H^+ \rightarrow HO_2^{\bullet} \quad (10)$$

$$HO_2^{\bullet} + HO_2^{\bullet} \rightarrow H_2O_2 + O_2 \quad (11)$$

According to the analysis above on the behavior of light irradiation, a combined effect functions in our photo-assisted electrochemical system through a series reactions between electrochemistry and photochemistry, and the synergy of combining the two advanced oxidation processes will be discussed in our following articles.

3.7. Stability and reusability of BFO catalyst

The stability and recyclability of BFO catalyst was evaluated by successive batches of 1,2,4-Acid degradation. After reaction, the suspension was centrifuged and the catalyst of BFO was separated and dried, then reused in the next round. The results shows that BFO catalyst was able to be reutilized for at least three cycles and the reused catalyst almost retained the catalytic activity as efficient as the fresh one (Fig. 7). No leaching of Fe and Bi ions from BFO catalyst was detected during the MB degradation at pH 5.0 by ICP-MS. The good chemical stability of BFO catalyst has verified its probable application in real industrial plants in a large scale. The good chemical stability of BFO was further confirmed by XPS measurements on the degradation before and after the 1,2,4-Acid degradation (data not shown), the XPS envelops of Fe 2p, Bi 4f and O 1s on the surface of the used catalyst were almost the same as that on the surface of the fresh one.

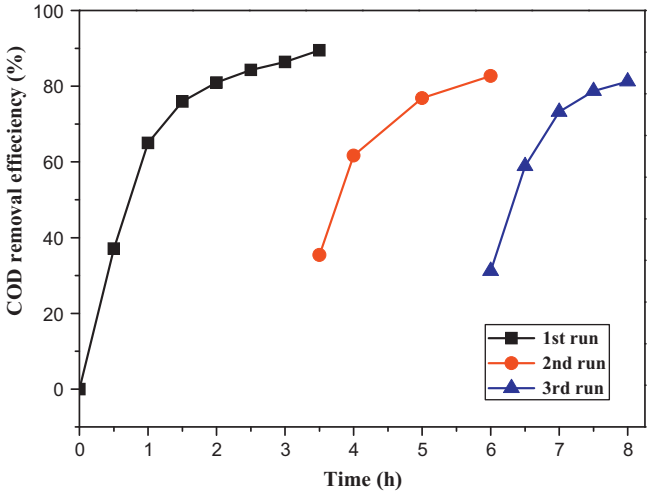

Fig. 7. Cycling runs in the degradation of 1,2,4-Acid in combined electrochemical degradation of 1,2,4-Acid with BFO particles. Conditions: $T = 25\,^{\circ}C$; Initial pH 5; electrode distance = 30 mm; Current density = 40 mA cm^{-2}; BFO dosage = 1 g L^{-1}.

Table 2
Accurate masses obtained from the UPLC-(ESI)-TOF-HRMS analysis of 1,2,4-Acid degradation products in the combined electrochemical process.

Compound	Formula	Retention time (min)	Detected (*m*/*z*)	Error (mDa)
1-diazo-2-naphthol-4-sulfonic acid	$C_{10}H_6N_2O_4S-$	11.37	247.981	−1.1
4-hydroxynaphthalene-1-sulphonic acid	$C_{10}H_8O_4S-$	9.74	220.140	1.4
1,2-Dihydronaphthalene	$C_{10}H_8O_2-$	10.61	249.768	0.2
1,2-naphthoquinone	$C_{10}H_6O_2-$	12.33	247.103	1.1
o-phthalic acid	$C_8H_6O_4-$	6.33	165.018	0.2
1,2-benzenedicarboxylic	$C_8H_4O_3-$	7.19	147.008	0.2
Benzoic acid	$C_7H_6O_2-$	6.79	121.442	−0.1
Hydroxybenzene	C_6H_6O-	4.61	93.034	−0.2
Maleic acid	$C_4H_4O_4-$	2.08	115.402	0.5
Ethanedioic acid (Oxalic acid)	$C_2H_2O_4-$	1.67	88.987	0.1
Acetic acid	$C_2H_4O_2-$	1.92	59.211	0.6
Methanoic acid (formic acid)	CH_2O_2-	0.79	44.997	−1.5

3.8. Mineralization of 1,2,4-Acid in the combined process

To verify the mineralization during the degradation of 1,2,4-Acid in combined electrochemical degradation with BFO particles, UPLC-(ESI)-TOF-HRMS was applied to detect the main intermediates during the process. In the analysis of intermediates in wastewater samples, UPLC-TOF chromatograms were recorded containing full scan spectral data. Degradation samples corresponding to $t = 0$, 20, 90, 150 and 200 min were taken to detect oxidation intermediates and to characterize their evolution with reaction time. A large number of different aromatic compounds were found by means of the UPLC-MS technique, and 11 of them were identified based on accurate mass measurements. The proposal of the best chemical structures was supported on prior knowledge of the molecule pattern and the oxidative treatment. Table 2 shows data related to the experimental and calculated masses of the deprotonated ions (mass to charge ratio; *m*/*z*), and the proposed empirical formula corresponding to the identified compounds. In all cases, the resulting accurate masses were found with an error lower than 1.9 mDa or 3.4 ppm. The tentative molecular structures and proposed degradation pathway are shown in Fig. 8.

With the available information, it is not possible to exactly know the molecular structures and differences between the detected intermediates. Fig. 8 only gives indications of the general structure that could justify MS data. To reveal the precise structures, more analysis, e.g., comparison with commercial standards (if available), Nuclear Magnetic Resonance (NMR), and or further tandem Mass Spectrometry (MS/MS) detection would be necessary. The identified intermediates appeared neither in all collected samples nor with the same time profile. The order of appearance of those intermediates helps to envisage the 1,2,4-Acid degradation mechanism in combined electrochemical process. Hydroxyl radicals, the main oxidant species involved in combined electrochemical oxidation process with BFO, are strong electrophilic oxidants. Consequently, 1,2,4-Acid reactive azo dye degradation should be initialed by the attack of HO• upon an electron-rich site, i.e., near the nitrogen atoms of the azo group [28].

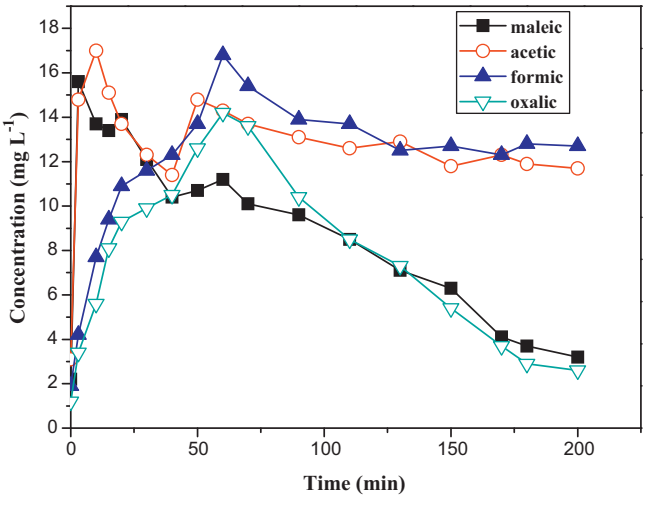

Fig. 8. Evolution of organic acids identified in 1,2,4-Acid oxidation by combined electrochemical process.

In view of this, the fast degradation of the dye solution seems to suggest a sequenced oxidation mechanism in which hydroxyl radical preferably attacks the chrophore center of the dye molecules (i.e., the azo groups, —N=N—) cleaving them into the two lateral substituted naphthalene rings. The non-detection of intermediates containing the original azo groups also points this direction. Azo groups may be attacked at two positions. One is at the C—N single bond between the azo group and the naphthalene ring, generating N_2 gas according to Eqs. (12) and (13) [29,30].

$$R{-}N{=}N{-} + HO^{\bullet} \rightarrow R{-}N{=}N^{\bullet} \quad (12)$$

$$R{-}N{=}N^{\bullet} \rightarrow R^{\bullet} + N{\equiv}N \quad (13)$$

The naphthalene ring would be the target of the nest HO• attack. Alternatively, the addition of HO• to one of the carbon atoms bearing the release of sulfonic groups from naphthalene ring, thus SO_4^{2-} presence on solution would clearly increase after the concentration of those intermediate began to decline (data not shown). On the other hand, the 1,2-benzenedicarboxylic, o-phthalic acid, hydroxybenzene show the direct addition of HO• to unsaturated aromatic bonds of the naphthalene structures, giving place to the formation of mono- or poly-hydroxylated derivatives. Further oxidation of those groups leads to the ring opening of benzene compounds. As stated in the literature, benzene and naphthalene group hydroxylation ends up with the ring opening, giving short chain carboxylic acids [29,31]. In the present study, formic, acetic, oxalic, and maleic acids were detected in solution and the evolution of their concentration with time is shown in Fig. 8. As can be seen, all carboxylic acid appear at the outset of the electrochemical degradation process. Acetic acid as an initial intermediate of the degradation of 1,2,4-Acid, reached a maximum concentration around $t = 10$ min and underwent a slight increase at the time of 40–50 min. The interesting phenomenon of fluctuations of acetic acid might be due to the different generation pathway. The formation of acetic acid would involve the oxidation of maleic acid and malonic acid [32]. Formic acid and acetic acid are the main oxidation products of maleic acid identified. However, maleic acid can also give rise to malonic acid, which would be continuously been oxidized to acetic acid. It might be a fact that suggests the increase of acetic acid concentration at near 40 min, in accordance with the previous studies that report the Fenton's degradation of 2,6-dimethylaniline [23].

This behavior is indicative of the fast and easy hydroxylation of the naphthalene and/or benzene rings in this combined oxidative

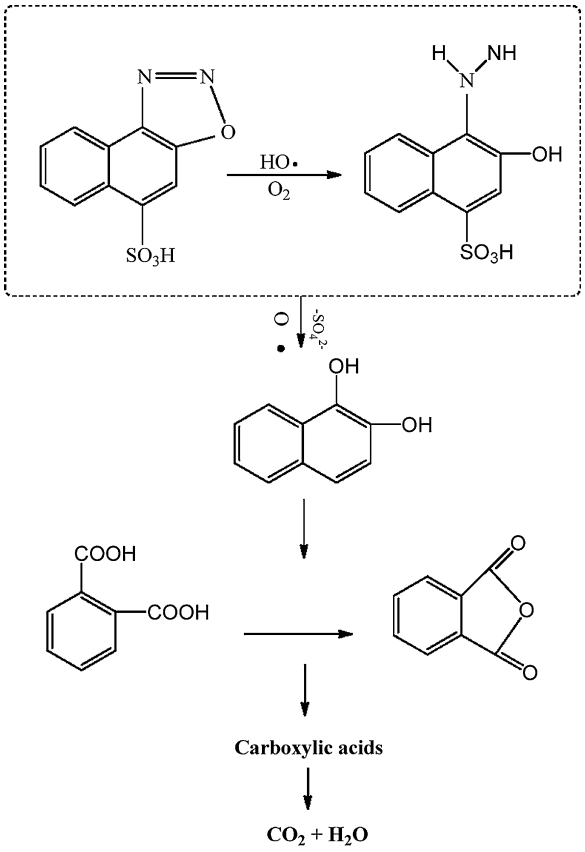

Fig. 9. Proposed reaction mechanism for1,2,4-Acid degradation in combined electrochemical process in the presence of BFO.

process. As previously known [29], some small molecular organic acids like acetic acid is quite resistant to the hydroxyl radical attack and its degradation requires longer reaction time.

This is consistent with the results obtained from the COD removal, however, in electrochemical systems with BFO, these acids might have more inclination to be absorbed on the surface of catalyst and make the concentrations of their by-product lower than the other literature reported [33]. Overall, the whole 1,2,4-Acid degradation by combined electrochemical process in the presence of BFO can be described by a series of consecutive steps, schematically depicted in Fig. 9.

3.9. FT-IR spectra study

FT-IR spectra for synthetic BFO, those adsorption of 1,2,4-Acid and after the degradation (100 min and 200 min) were recorded (Fig. 10) in order to investigate the evolution of functional groups on the surface of 1,2,4-Acid. As shown in Fig. 10, two strong absorptions were observed around 443 and 553 cm^{-1} in the FT-IR spectrum of BFO, indicating O—Fe—O bending vibrations and Fe—O stretching of FeO_6 groups in perovaskite BFO, respectively.

As shown in Fig. 10(a), dominated peaks of 1,2,4-Acid all appears indicating a good adsorption properties of BFO, such as the stretching vibration of —OH (3728 cm^{-1}), C—C bond of the naphthalene ring (1523 cm^{-1}), bending vibration of =C—H (198—1255 cm^{-1}), —N=N—O— of the naphthalene ring (1447 cm^{-1}), characteristic peak of C—N vibration (1366 cm^{-1}), —SO_3H (1207 cm^{-1}) and symmetrical stretching vibration of C—S—O at 770 cm^{-1}. The 100min's spectra of BFO after electrochemical degradation are shown in Fig. 10(c), the naphthalene ring vibration characteristic peaks almost disappeared after 100 min reaction, indicating a ring opening reaction occurred in this stage. The peak about 1124 cm^{-1}

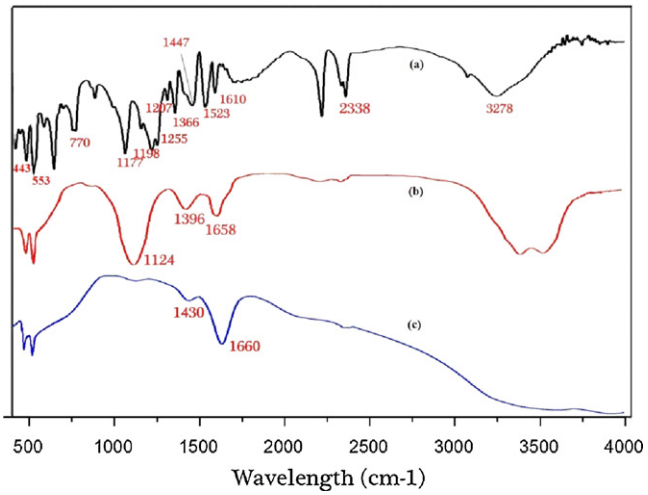

Fig. 10. FT-IR spectra of BFO particles collected during the electrochemical degradation process. (a) After adsorption of 1,2,4-Acid; (b) after 100 min oxidation; (c) after 200 min oxidation.

assigned to antisymmetric stretching vibration of SO_4^{2-}, suggesting the oxidation of naphthalene-sulfonate group. Moreover, some new peaks are found in curve (b) including stretching vibration of C=O (1658 cm^{-1}), symmetric stretching vibration of COO— (1396 cm^{-1}), further indicating the opening of aromatic ring to generating substance like polycarboxylate. A further degradation after 200 min IR spectra of BFO is shown in Fig. 10(c), that characteristic peaks of naphthalene thoroughly disappeared, only leaving some groups of stretching group of C=O (1660 cm^{-1}) and carboxylate ions (1430 cm^{-1}), which were believed to belong to functional groups of low molecular acids, thus indicating a mineralization of 1,2,4-Acid on the surface of BFO particles but not only a adsorption effect occurred.

3.10. Proposed catalytic mechanism

Multi-phased electrochemical oxidation of 1,2,4-Acid with BFO is dependent on the role of electrolysis, BFO adsorption and their interaction. The mineralization of the organic compounds in this system is assumed to be initialed by the hydroxyl radicals attacking. The overall reaction equation should be summarized as Eq. (14).

$$C_{10}H_6N_2O_4S\underline{HO}{\cdot}10CO_2 \uparrow + 3H_2O + N_2 \uparrow + SO_4^{2-} \quad (14)$$

Under acidic or neutral conditions, the mechanism of the electro-generated H_2O_2 activation is probably initialed by the BFO particles. This may involve the initial formation of a complex between ≡Fe(III) and H_2O_2, where ≡Fe(III) stands for Fe(III) sites on the catalyst surface. The initially generated ≡Fe(III)H_2O_2 species are converted to ≡Fe(II) species and $^{\bullet}HO_2$, and the generated $^{\bullet}HO_2$ may further react with ≡Fe(III) to produce ≡Fe(II) species. All the formed ≡Fe(II) can react with H_2O_2 to generate •OH radicals. The mechanism is consistent with the observations on the literature [34,35]. According to the above discussion, it is thought that •OH radicals make a major contribution in the degradation of 1,2,4-Acid at pH 5. Thus, the degradation of •OH radicals was monitored by using ESR in this electrochemical combined process. The EPR spectrum in the three different systems displayed a 4-fold characteristic peak of the typical DMPO-•OH adduct. Weak •OH and $^{\bullet}O_2H$ signals were observed in the only BFO or electrochemical existed system (Fig. 11(a) and (b)), as compared, the DMOP-•OH signals became stronger when the combined system was introduced, indicating a BFO induced production of hydroxyl radicals occurred. The results clearly suggest that an interaction occurred between BFO particles and electrochemical process.

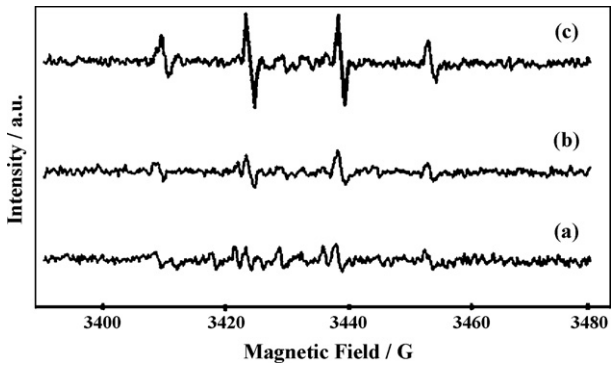

Fig. 11. DMPO spin-trapping ESR spectra of •OH radicals in the systems of (a) BFO (b) electrochemical (c) combined electrochemical process with BFO. Conditions: Initial pH 5; electrode distance = 30 mm; Current density = 40 mA cm^{-2}; BFO dosage = 1 g L^{-1}.

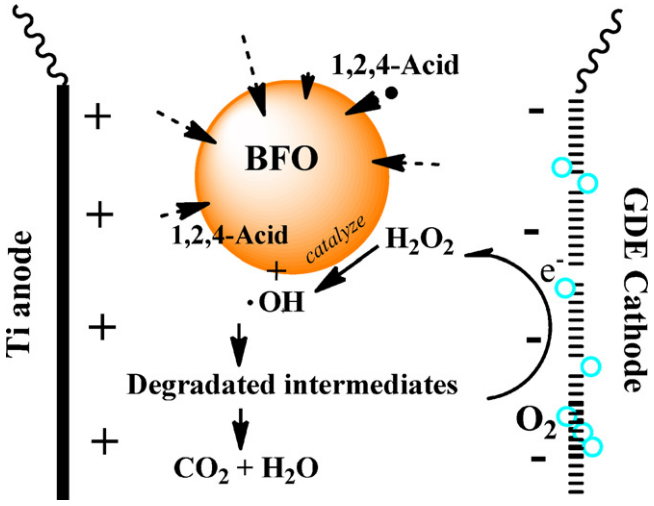

Fig. 12. Diagram of the proposed mechanism of combined electrochemical oxidation process in the presence of BFO catalyst.

As it is mentioned above, the whole process may involve the following 3 steps:

(a) 1,2,4-Acid mass transferred onto the surface of BFO particles;
(b) Electro-generated hydrogen peroxide was decomposed via the active part on the BFO particles forming the strong oxidant •OH radicals.
(c) The pollutants were attacked by the hydroxyl radicals and finally eliminated.

To gain further insights into the catalytic effect of BFO in the electrochemical combined system, the main reaction mechanism of catalytic oxidation of pollutant was depicted in Fig. 12.

4. Conclusions

Spinal-like $Bi_2Fe_4O_9$ showed an excellent catalytic activity for the degradation of 1,2,4-Acid at neutral pH in the electrochemical system using a gas diffusion cathode fed with air. The results of the bulk electrolysis under different experimental conditions showed that 1,2,4-Acid was destroyed completely in the BFO combined electrolytic system. The oxidation rate can be affected by the current density, the solution pH and dosage of catalyst. The UPLC-(ESI)-TOF-MS technique was used to detect the main intermediates that might be produced through the degradation. 11 of them were detected with some short chain carboxylic acids at long reaction times, as a previous step to complete mineralization. The mechanism of this combined system was proposed and verification by the ESR technique, the results showed that the 1,2,4-Acid elimination was the result of acid oxidation by hydroxyl radical oxidation produced by the decomposition of electro-generated H_2O_2. Hydroxyl radicals were assumed to be the main oxidant and played a key role in the removal of organic pollutants in this combined system.

Acknowledgement

We thank the Shanghai Scientific Committee for financial support (Project NO. 10dz120010b). The help of Instrument of Analysis Center of SJTU with the analysis of samples is greatly acknowledge.

References

[1] C. Pulgarin, R.A. Torres-Palma, J.I. Nieto, E. Combet, C. Petrier, Water Res. 44 (2010) 2245–2252.
[2] R.A. Torres-Palma, R.E. Palma-Goyes, F.L. Guzman-Duque, G. Penuela, I. Gonzalez, J.L. Nava, Chemosphere 81 (2010) 26–32.
[3] R.M. Quinta-Ferreira, R.C. Martins, A.M.T. Silva, S. Castro-Silva, P. Garcao-Nunes, Environ. Technol. 32 (2011) 1031–1041.
[4] J.Z. Li, M. Tian, C. Niu, X.Y. Yuan, X.Y. Chen, Conference on Environmental Pollution and Public Health 1–2 (2010) 1118–1122.
[5] L. Gherardini, C. Comninellis, N. Vatistas, Ann. Chim. (Rome) 91 (2001) 161–168.
[6] P. Canizares, C. Saez, J. Lobato, M.A. Rodrigo, Electrochim. Acta 49 (2004) 4641–4650.
[7] M. Panizza, G. Cerisola, Water Res. 43 (2009) 339–344.
[8] M.A. Oturan, I. Sires, J.A. Garrido, R.M. Rodriguez, E. Brillas, N. Oturan, Appl. Catal. B: Environ. 72 (2007) 382–394.
[9] E. Brillas, R. Sauleda, J. Casado, J. Electrochem. Soc. 145 (1998) 759–765.
[10] E. Garrido-Ramirez, M.S. Ureta-Zanartu, M.D. Mora, Abstr. Pap. Am. Chem. Soc. 241 (2011).
[11] M.H. Zhou, W. Wang, Q.O. Mao, J.J. Yue, X. Wang, Catal. Commun. 11 (2010) 937–941.
[12] B.H. Hameed, N.K. Daud, Desalination 269 (2011) 291–293.
[13] C. Moreno-Castilla, M.A. Fontecha-Camara, M.A. Alvarez-Merino, F. Carrasco-Marin, M.V. Lopez-Ramon, Appl. Catal. B: Environ. 101 (2011) 425–430.
[14] Y.H. Chu, L.W. Martin, Q. Zhan, P.L. Yang, M.P. Cruz, K. Lee, M. Barry, S.Y. Yang, R. Ramesh, Ferroelectrics 354 (2007), 167-+.
[15] M.S. Awan, A.S. Bhatti, J. Mater. Eng. Perform. 20 (2011) 283–288.
[16] B. Wang, L. Gu, H.Z. Ma, J. Hazard. Mater. 143 (2007) 198–205.
[17] G.Q. Zhang, S. Zhao, L. Fu, L.F. Liu, X.H. Fang, F.L. Yang, Electroanalysis 23 (2011) 355–363.
[18] A.T. Bell, Science 299 (2003) 1688–1691.
[19] L.H. Zhu, W. Luo, N. Wang, H.Q. Tang, M.J. Cao, Y.B. She, Environ. Sci. Technol. 44 (2010) 1786–1791.
[20] T.D. Waite, C.K. Duesterberg, S.E. Mylon, Environ. Sci. Technol. 42 (2008) 8522–8527.
[21] M.H. Zhou, Q.H. Yu, L.C. Lei, G. Barton, Sep. Purif. Technol. 57 (2007) 380–387.
[22] M.C. Lu, N. Masomboon, C. Ratanatamskul, Environ. Sci. Technol. 43 (2009) 8629–8634.
[23] M.C. Lu, N. Masomboon, C. Ratanatamskul, J. Hazard. Mater. 176 (2010) 92–98.
[24] P.R. Gogate, A.B. Pandit, Adv. Environ. Res. 8 (2004) 501–551.
[25] H. Zhang, D.B. Zhang, J.Y. Zhou, J. Hazard. Mater. 135 (2006) 106–111.
[26] J.M. Liu, F. Gao, X.Y. Chen, K.B. Yin, S. Dong, Z.F. Ren, F. Yuan, T. Yu, Z. Zou, Adv. Mater. 19 (2007) 2889–2892.
[27] J.H. Ma, W.J. Song, C.C. Chen, W.H. Ma, J.C. Zhao, Y.L. Tang, Environ. Sci. Technol. 39 (2005) 5810–5815.
[28] C. Galindo, P. Jacques, A. Kalt, J. Photochem. Photobiol. A 130 (2000) 35–47.
[29] M. Karkmaz, E. Puzenat, C. Guillard, J.M. Herrmann, Appl. Catal. B: Environ. 51 (2004) 183–194.
[30] H. Lachheb, E. Puzenat, A. Houas, M. Ksibi, E. Elaloui, C. Guillard, J.M. Herrmann, Appl. Catal. B: Environ. 39 (2002) 75–90.
[31] M. Stylidi, D.I. Kondarides, X.E. Verykios, Appl. Catal. B: Environ. 40 (2003) 271–286.
[32] J.J. Rodriguez, J.A. Zazo, J.A. Casas, A.F. Mohedano, M.A. Gilarranz, Environ. Sci. Technol. 39 (2005) 9295–9302.
[33] M.C. Lu, N. Masomboon, C. Ratanatamskul, Appl. Catal. A: Gen. 384 (2010) 128–135.
[34] C.M. Miller, R.L. Valentine, Water Res. 33 (1999) 2805–2816.
[35] W.P. Kwan, B.M. Voelker, Environ. Sci. Technol. 37 (2003) 1150–1158.